



Substorm plasma sheet ion pressure profiles

Simon Wing,¹ Jesper W. Gjerloev,¹ Jay R. Johnson,² and R. A. Hoffman³

Received 20 April 2007; revised 13 June 2007; accepted 1 August 2007; published 29 August 2007.

[1] The plasma sheet pressure, temperature, and density profiles inferred from DMSP observations are used to investigate substorm growth, expansion, early-recovery, and late-recovery phases. During the growth phase, the pressure peaks at the inner edge of the plasma sheet. The premidnight pressure peak is associated with the temperature peak, while the postmidnight peak is associated with the density enhancement. After the substorm onset, the pressure at the inner edge diminishes. Instead, the pressure peaks at premidnight from $X = -10$ to $-40 R_E$, which can be associated with temperature enhancement. During the early and late recovery phases, the pressure peaks at postmidnight, which is associated with a cold, dense ion population, possibly resulting from ion outflow and the substorm current systems. In the near-Earth region, the entropy decreases after substorm onset, but the specific entropy appears to be roughly conserved.
Citation: Wing, S., J. W. Gjerloev, J. R. Johnson, and R. A. Hoffman (2007), Substorm plasma sheet ion pressure profiles, *Geophys. Res. Lett.*, *34*, L16110, doi:10.1029/2007GL030453.

1. Introduction

[2] The substorm is one of the most interesting and complex phenomena in space physics. Its development has generally been categorized into three phases: growth, expansion, and recovery. The growth phase is typically defined as the quiescent period starting at the time of the southward turning of the Interplanetary Magnetic Field (IMF) and ending at the onset of the expansion phase (commonly referred to as the substorm onset). During the growth phase, the auroral oval expands equatorward, the aurora and the electrojet gradually intensify, the plasma sheet thins, and the magnetospheric magnetic field lines stretch (become tail-like) as the solar wind energy is stored in the magnetotail. The growth phase is followed by the expansion phase, during which the auroral oval expands poleward, eastward, and westward, and the magnetic field configuration in the inner plasma sheet changes rapidly from the stretched tail-like to a more dipolar configuration. The expansion phase is followed by the recovery phase, which corresponds to the return of the magnetosphere to the undisturbed state. A more detailed description of substorm phases is given by *Lui* [1991].

[3] The present study investigates the plasma sheet density, temperature, and pressure profiles during the following

substorm phases: growth, expansion, early recovery, and late recovery.

2. Substorm Event Selections

[4] The selection of the substorm events included in the present study was based on both the optical characteristics and the AL index pattern. The selected events satisfy the following criteria: (1) fairly isolated optically and magnetically; (2) poleward expansion from a localized onset; (3) a single expansion and recovery phase (in case of a secondary expansion, the event end is defined as the end time of the second expansion); (4) the entire auroral bulge region, and preferably most of the oval, is in darkness; and (5) magnetic storms ($Dst < -30$) or periods of long magnetic activity are excluded.

[5] The requirement of a localized onset in the nighttime hours and the bulge-type event eliminates other types of disturbances such as the shock or pressure pulse auroras. In all, a total of 180 substorm events were selected for the present study.

[6] The substorm phases were normalized by the onset of brightening (T_0) and the peak of the substorm (T_1). The selection of these times was based purely on the global auroral images. Utilizing both the Polar VIS Earth Camera and the Polar UVI enables us to determine the onset time to within 1 min, which is sufficiently accurate for the present study. The substorm maximum or end of the expansion phase (T_1) is based on a qualitative estimate of the time at which the combined optical emission intensity and the poleward expansion of the aurora are or near maximum. The intensity often begins to fade before the expansion ceases, especially at the end of the bulge [*Gjerloev et al.*, 2007]. Thus the selection of the global aurora maximum or peak incorporates optical characteristics. In agreement with the more classical definition of the peak, *Gjerloev et al.* [2007] show that this technique results in the maximum substorm time that coincides with the average minimum AL. The duration of the expansion phase is defined as $\Delta t = T_1 - T_0$. Δt ranges from 7 to 92 min with a median of 32 min and a mean of 35 ± 18 min. The four phases analyzed in this study are (1) $(\text{onset} - \Delta t) \leq \text{growth phase} < \text{onset}$, (2) $\text{onset} \leq \text{expansion phase} < (\text{onset} + \Delta t)$, (3) $(\text{onset} + \Delta t) \leq \text{early recovery phase} < (\text{onset} + 2\Delta t)$, and (4) $(\text{onset} + 2\Delta t) \leq \text{late recovery phase} < (\text{onset} + 3\Delta t)$.

3. DMSP Data

[7] The DMSP SSJ4 instrument measures only highly field-aligned precipitating particles at energy range of 32 eV to 30 keV at an altitude of roughly 835 km. Plasma sheet ions have been observed to be nearly isotropic irrespective of the activity levels [e.g., *Kistler et al.*, 1992]. Taking advantage of these properties, *Wing and Newell* [1998] have

¹Johns Hopkins University Applied Physics Laboratory, Laurel, Maryland, USA.

²Princeton Plasma Physics Laboratory, Princeton, New Jersey, USA.

³Space Weather Laboratory, NASA Goddard Space Flight Center, Greenbelt, Maryland, USA.

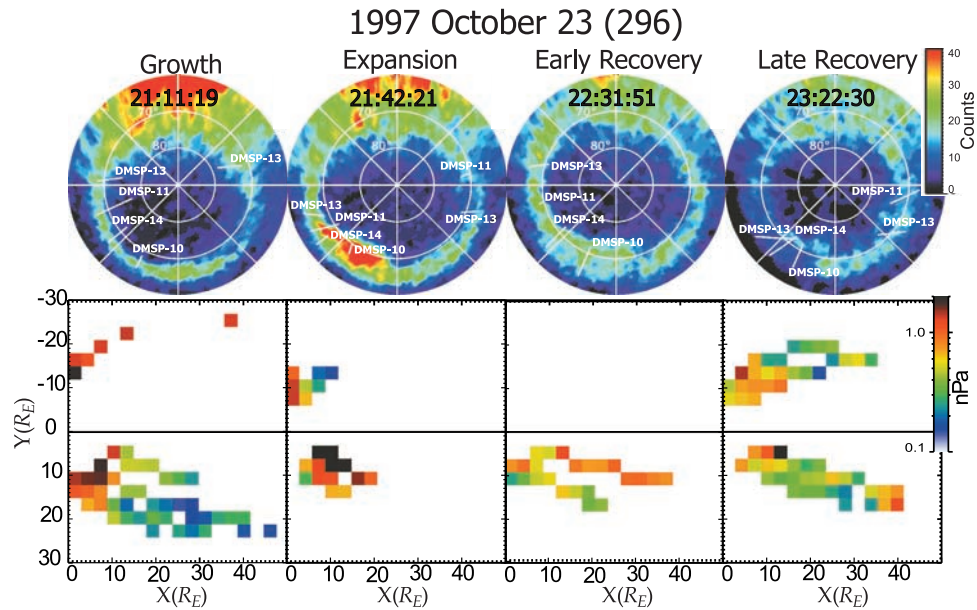


Figure 1. An example substorm occurring on October 23, 1997. (top) VIS Earth Camera images (124–149 nm) obtained during the four substorm phases with DMSP passes superposed. Noon is at the top and midnight at the bottom. (bottom) Equatorial pressure inferred from DMSP observations.

developed a method for inferring the plasma sheet ion temperature, density, and pressure from the DMSP SSJ4 measurements. The present study uses essentially the same method, which has been fully described by *Wing and Newell* [1998], with the following modifications deemed necessary for substorm studies.

[8] As noted in section 1, the topology of the magnetospheric magnetic field changes rapidly during the evolution of the substorm loading-unloading cycle. This complicates the ionosphere-plasma sheet mapping. Instead of using the real values of b_2i and K_p as inputs to the modified T89 magnetic field model [Tsyganenko, 1989], as done by *Wing and Newell* [1998], we utilized the original unmodified T89 with the following caveat. The K_p input to the T89 was fixed to 4, 1, 2, and 2 for growth, expansion, early recovery, and late recovery phases, respectively. We believe that the resulting T89 magnetic field line would more closely resemble the well-known magnetic field configurations during these substorm phases. *Opgenoorth et al.* [1994] compares the disturbed-time ionosphere-to-equatorial plane mapping of the original T89, which does not have field-aligned currents (FAC), with that of T89 + FAC. The study finds that the two methods result in locations that differ by a few R_E in the equatorial plane [Opgenoorth et al., 1994, Figure 6]. *Pulkkinen and Tsyganenko* [1996] also evaluates the ionosphere-to-equatorial plane mapping in T89, which is symmetrical with respect to midnight meridian, and finds the errors for points originating in the auroral oval to be within a few R_E in the X or Y direction (see also *Wolf et al.* [2006] for evaluating entropy with T89). In light of these estimated mapping uncertainties and the limited number of events, we averaged the pressures, densities, and temperatures in $3 \times 3 R_E^2$ bins. The difficulty of accurate ionosphere-magnetosphere mapping is certainly a concern in the present study, which limits the results to only the large-scale spatiotemporal behavior of the fundamental plasma sheet parameters.

[9] Another important aspect of this method is that instead of computing moments, which is commonly done, each ion spectrum is fitted to distribution functions (one-component Maxwellian, two-component Maxwellian, and κ), and the best fit is selected. This takes into account ions outside the detectors' energy range. Therefore, the densities obtained can be larger than those calculated using moments. Moments may also underestimate temperatures by ignoring the hotter components (when they are significant), which may explain some of the temperature differences resulting from using the two methods. Electron acceleration (inverted V) events, which usually indicate the presence of significant field-aligned electric field, were eliminated from our database.

[10] Five DMSP satellites were operational in the 1997–2001 interval, F10, F11, F12, F13, and F14. Out of the 180 substorm events, 132 events have simultaneous DMSP particle observations. Figure 1 shows an example from October 23, 1997 event. The top row displays the Polar VIS Earth Camera images obtained during the four above-defined substorm phases. The DMSP passes are superposed onto the Polar VIS images, showing the locations of the ion data used to infer the equatorial plasma sheet pressure shown at the bottom row.

4. Plasma Sheet Ion Pressure Profiles During Substorm

[11] Figures 2a–2d show the inferred plasma sheet ion pressure profiles in the equatorial plane during substorm growth, expansion, early recovery, and late recovery phases, respectively, while Figures 2e–2h and 2i–2l present the corresponding density and temperature profiles, respectively. White space denotes either a data gap or a bin with less than four data points. Sections 4.1 to 4.4 summarize key features of Figure 2 during the four substorm phases. Although there are limitations to the data coverage and technique, the

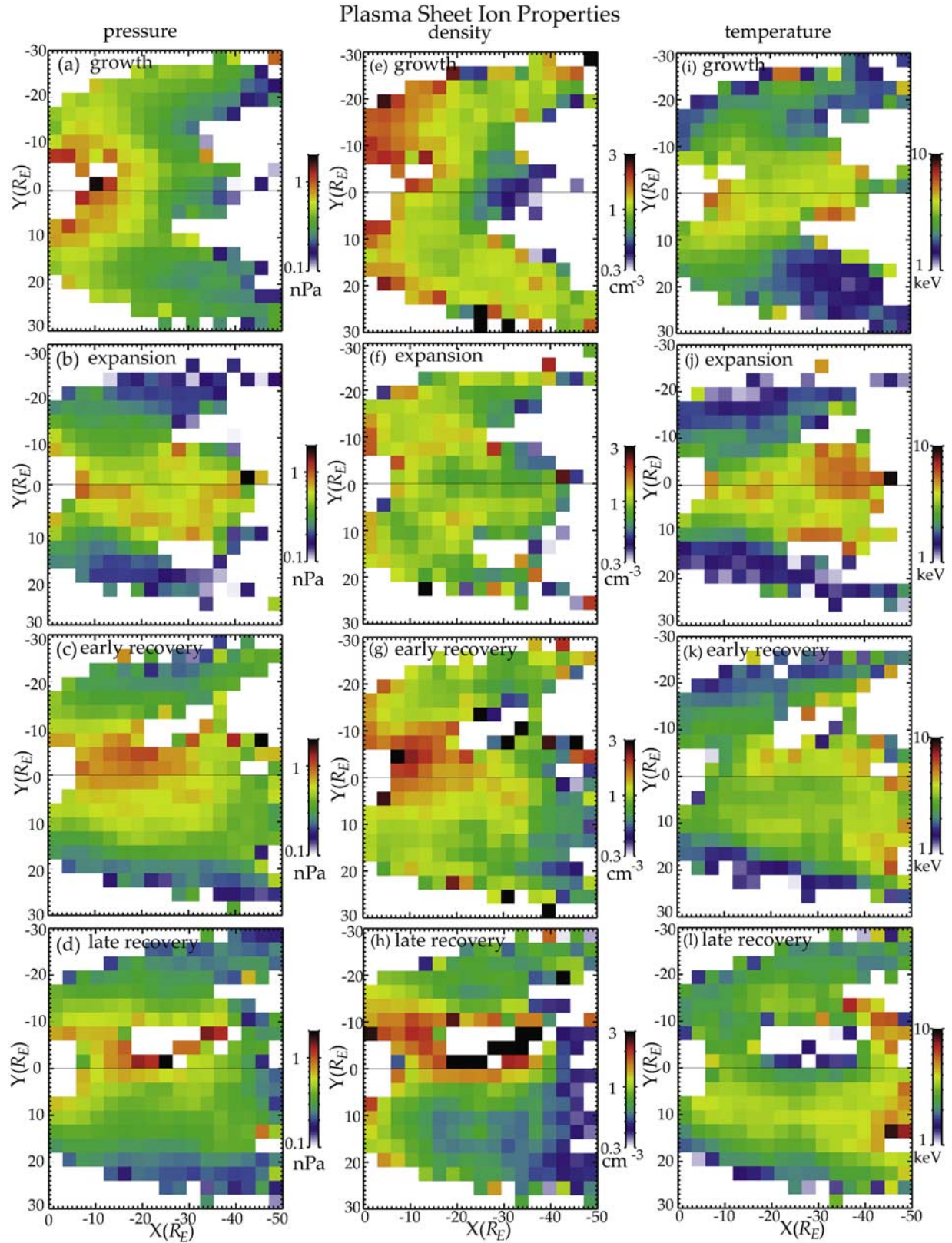


Figure 2. (a–d) Average equatorial pressure profiles inferred from DMSP observations during growth, expansion, early recovery, and late recovery phases, respectively, and their corresponding (e–h) density and (i–l) temperature profiles.

patterns, nonetheless, reveal some intriguing large-scale features.

4.1. Growth Phase

[12] (1) The pressure peaks at the inner edge of the plasma sheet (Figure 2a). (2) The premidnight pressure peak is associated with enhanced temperatures, whereas the postmidnight peak is associated with enhanced densities (Figures 2i and 2e).

4.2. Expansion Phase

[13] (1) Compared with the growth phase values, the pressure diminishes at the inner edge. (2) The pressure peaks at premidnight (Figure 2b, $X \in [-10, -40] R_E$, $Y \in [0, 10] R_E$), which is primarily associated with a temperature enhancement (Figure 2j). (3) Near the midnight meridian, at the inner edge, the density decreases, while at the mid-tail region, the density increases from values at the growth phase (Figures 2e and 2f).

4.3. Early Recovery Phase

[14] (1) The pressure peaks at postmidnight ($X \in [-10, -40] R_E$, $Y \in [-10, 0] R_E$), which is mainly associated with a density enhancement (Figures 2c and 2g). (2) Compared with the expansion phase, the temperatures in the midnight region ($X \in [-10, -40] R_E$, $Y \in [-10, 10] R_E$) have decreased, but the densities have increased.

4.4. Late Recovery Phase

[15] (1) The postmidnight pressure peak persists or may even become stronger in some localized regions ($X \in [-10, -40] R_E$, $Y \in [-10, 0] R_E$) while the premidnight pressures have decreased from the early recovery phase values. (2) The pronounced postmidnight pressure peak is associated with a cold, dense ion population (Figures 2d, 2h, and 2l). (3) The premidnight pressure decline from the early recovery phase coincides with the disappearance of the premidnight density enhancements (Figures 2g and 2h). (4) The premidnight pressure has generally decreased, while the near-midnight temperatures have also decreased below the expansion phase values.

[16] Note that in Figure 2 the equatorial data coverage provided by individual events is insufficient to address the spatiotemporal behavior of the parameters in the entire plasma sheet. However, a careful analysis of individual events supports the large-scale behavior described above.

5. Discussion and Summary

[17] The pressure, density, and temperature peaks at the inner edge of the plasma sheet during the growth phase are consistent with the previous DMSP observations for the active time plasma sheet [e.g., *Wing and Newell*, 1998]. The calculations by *Spence and Kivelson* [1993] show that while $\mathbf{E} \times \mathbf{B}$ convection moves ions of all energies sunward, the curvature and gradient drift moves hotter ions duskward, leading to a temperature peak in the dusk-midnight sector at the inner edge of the plasma sheet, in agreement with Figure 2i. The growth phase postmidnight pressure peak is associated with the density peak, which is consistent with the previously reported active time plasma sheet density and pressure profiles [*Wing and Newell*, 1998] and in situ observations at geosynchronous orbit [*Korth et al.*, 1999].

At the inner edge of the dawn plasma sheet, during the growth phase, the $\mathbf{E} \times \mathbf{B}$ earthward convection is countered by the curvature/gradient drift, which results in a stagnation point leading to the density buildup at the dawnside. This can be seen in the Alfvén layer calculations by *Friedel et al.* [2001] and the ion flow pattern in *Wang et al.* [2004] model calculations. These theoretical predictions and the observations are in good agreement with the asymmetric distributions seen in Figures 2e and 2i.

5.1. Entropy Before and After Substorm Onset

[18] At the substorm onset, there is a large-scale dynamic transition in the magnetospheric state as energy stored in the tail is released and the magnetic field dipolarizes. To gain insight regarding the dynamic process leading to the new state, we consider entropy prior to and after substorm onset. Nonconservation of entropy results from nonadiabatic processes, e.g., turbulent transport, thermal energy transport due to nonadiabatic particle drifts, or precipitation, and may indicate which processes are most important in the transition to the new state of the system. Although such comparisons may not necessarily identify a substorm trigger, they do raise some important issues.

[19] In the case where mass is conserved on a flux tube and there is no heat loss, a useful conserved quantity is $S = \int p^{1/\gamma} ds/B$, where p = the plasma pressure, B = magnetic field, γ = the polytropic index ($= 5/3$). Although not precisely the entropy of the flux tube, this quantity is entropy-like in nature [*Birn et al.*, 2006]. For isotropic pressure (as assumed in our mapping) and the system near equilibrium in the initial and final configuration, the pressure is constant along field lines, and entropy (S) $\sim p^{1/\gamma} V$ (V is flux tube volume). This extensive parameter is proportional to system size.

[20] To compare the entropy change in the transition from the growth phase to the expansion phase, we consider the flux tube volumes for field lines that share the same footpoint (point B) as shown in Figure 3. In doing so, we ignore the slow slippage of the footpoints on a convective time-scale. Using T89, point B is traced along the field line for $Kp = 4$ (growth phase; more stretched field lines) and $Kp = 1$ (expansion phase; more dipolarized field lines) to points A and C, respectively, on the equatorial plane (minimum $|\mathbf{B}|$), as sketched in Figure 3. Entropy is compared at these two different locations in the midnight meridian: at midtail region ($A = -30 R_E$, $C = -20 R_E$) and at near-Earth region ($A = -20 R_E$, $C = -7 R_E$). From the results displayed in Table 1, it is apparent that there is a substantial decrease in S (by a factor of 8) for dipolarized field lines in the near Earth region and a slight increase in S at the midtail region.

[21] The entropy reduction after substorm onset is consistent with previous Geotail observations [e.g., *Wolf et al.*, 2006]. It has been attributed to the combined effect of the plasma pressure (and density) decrease and dipolarization in the near-Earth region [e.g., *Lyons et al.*, 2003a]. The pressure and density decreases at the inner edge of the plasma sheet after substorm onset can be seen in Figures 2a, 2b, 2i, and 2j. Entropy reduction is also found in the simulation of *Birn et al.* [2006], where plasmoid formation in the tail leads to a decrease of S on field lines attached to Earth following reconnection (essentially by shedding the entropy carried in the plasmoid).

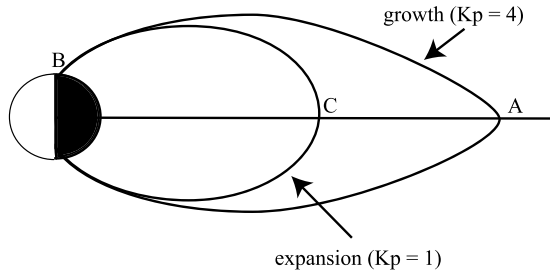


Figure 3. Schematic depicting the magnetic field line configurations for growth and expansion phases. See text for full explanations.

[22] It is also of interest to consider the relevance of our results on the convection model within each phase of the substorm. The growth phase might be expected to exhibit a steady-state convection. When comparing the entropy at two locations during the growth phase (-30 and $-20 R_E$), a decrease of S by a factor of 1.5 is found. This is to be contrasted with the decrease of S by a factor of 8 in the transition from growth phase to expansion phase. This result suggests that there may be a decrease of S during the growth phase, consistent with the finding of *Goertz and Baumjohann* [1991]. This reduction in S may be related to flux across field lines — for example, gradient and curvature drifts — that may also be related to the buildup in the pressure gradient, resulting in entropy loading of the dusk-side [*Lyons et al.*, 2003b].

[23] Finally, it is interesting to examine the specific entropy, p/ρ^γ , which is an intensive variable of the system and should not depend on the system size (e.g., flux tube volume). In this case, $p/\rho^\gamma \sim p/n^\gamma$ (assuming a single ions species) appears to be roughly conserved in the near-Earth region before and after onset (bottom row of Table 1). This result would be consistent with volume/mass reduction without significant plasma heating or heat flux, e.g., plasmoid. In contrast, there is a slight reduction of specific entropy in the midtail region.

[24] Another view of substorm expansion is that it occurs when field lines diffuse through a turbulent region. In this case, the particles/fluid are not frozen to the field lines and a decrease in entropy may be expected as the flux tube volume decreases and plasma is lost. However, it is uncertain whether the specific entropy would be conserved through such particle transport. Estimating how S would change for various candidate transport models, and whether specific entropy would remain relatively invariant compared with the significant loss of S , would be useful.

5.2. Recovery Phase Pressure Peak

[25] The substorm recovery phase is the least studied phase in substorms. An interesting finding in this study is that the ion pressure peak changes from premidnight in the expansion phase to postmidnight in the early and late recovery phases. The postmidnight peak appears to be stable well into the late recovery phase, in contrast with the premidnight pressure peak, which has a shorter lifetime. The different properties of the two peaks (cf. section 4), however, suggest that they are probably due to different processes, and hence the pressure peaks should not be viewed as moving from premidnight to postmidnight.

[26] The (early and late) recovery phase postmidnight pressure peak can be attributed to cold dense ions (Figures 2g, 2h, 2k, and 2l), which may result from the ion outflow after the substorm onset. Studies have shown that the ion outflow rate peaks about 20 to 30 min after substorm onset and remains at an elevated level up to 70 min or even beyond 90 min, depending on the methodology [e.g., *Wilson et al.*, 2004].

[27] Although various substorm-associated current systems have been proposed, the substorm current wedge [e.g., *McPherron et al.*, 1973] and the two-component westward electrojet (WEJ) system [e.g., *Kamide and Kokubun*, 1996] are two of the most well accepted. The cross-tail current is believed to be diverted through a downward FAC in the postmidnight region, closing in the auroral ionosphere by a WEJ and finally to an upward FAC in the premidnight region.

[28] Studies have shown that an increase in ionospheric ion outflow can be associated with increases in FAC [e.g., *Winglee et al.*, 2005] and upward FAC can drive O^+ upwellings [e.g., *Gombosi and Nagy*, 1989]. An increase in ion outflow, in turn, can lead to the observed plasma sheet density and hence to pressure enhancements. The resulting azimuthal pressure gradient can generate FAC [e.g., *Wing and Newell*, 2000]. The coupling or cycle of the pressure increase — FAC increase — ion outflow increase — density increase may self-feed and self-perpetuate. However, it is also possible that the resulting pressure gradient acts to inhibit FAC, e.g., by generating FAC with the opposite polarity. This needs to be further investigated. In the context of the results presented here it is nevertheless interesting that the postmidnight pressure enhancement in the late recovery phase is associated with cold, dense ions. This would be consistent with ionospheric ion outflow at this local time, which may be associated with FAC that is part of the substorm current wedge. However, the substorm current wedge is believed to be short lived and may play a role in the early recovery phase, but whether it plays any

Table 1. Flux Tube Volumes, Ion Pressure, Density, Entropy, and Specific Entropy (p/n^γ) for Growth and Expansion Phases in the Midnight Meridian^a

Substorm Phase	Location (X, Y, Z) R_E	Flux Tube Volume	Ion Pressure, nPa	$S = p^{1/\gamma} V$	Density, cm^{-3}	p/n^γ
Midtail						
Growth	A = (-30, 0, 0)	8724	0.31	4320	0.49	1.0
Expansion	C = (-20, 0, 0)	7899	0.55	5518	0.83	0.75
Near-Earth						
Growth	A = (-20, 0, 0)	3976	0.53	2717	0.89	0.65
Expansion	C = (-7, 0, 0)	379	0.90	356	1.2	0.66

^aPressures and densities from Figure 2 are averaged in $6 \times 6 R_E$ bin. See the schematic in Figure 3.

significant role in the late recovery phase as defined in this study is questionable [e.g., *Kamide and Kokubun*, 1996].

[29] The observations presented in this paper provide important constraints which various substorm theories must be able to account for.

[30] **Acknowledgments.** We acknowledge helpful discussions with Shin Ohtani and Kan Liou. Fred Rich has been helpful in obtaining DMSP SSJ4 data, as has the World Data Center in Boulder, Colorado. Simon Wing gratefully acknowledges the support of NASA Grants NNG04GN14G, NNX06AB87G, and NSF Grant ATM-0538513. Jesper Gjerloev gratefully acknowledges NASA grants LWS02-0000-0084 and SRT02-0000-0081. Jay Johnson acknowledges NASA grants NNH04AA731, NNH04AB231, and NNG06GE96G and NSF grant ATM-0411392.

References

- Birn, J., M. Hesse, and K. Schindler (2006), On the role of entropy conservation and entropy loss governing substorm phases, in *Proceedings of the Eighth International Conference on Substorms (ICS-8)*, edited by M. Syrjäsoo and E. Donovan, pp. 19–24, Univ. of Calgary, Calgary, Alberta, Canada.
- Friedel, R. H. W., H. Korth, M. G. Henderson, and M. F. Thomsen (2001), Plasma sheet access to the inner magnetosphere, *J. Geophys. Res.*, *106*, 5845–5858.
- Gjerloev, J. W., R. A. Hoffman, J. B. Sigwarth, and L. A. Frank (2007), Statistical description of the bulge-type auroral substorm in the far ultraviolet, *J. Geophys. Res.*, *112*, A07213, doi:10.1029/2006JA012189.
- Goertz, C. K., and W. Baumjohann (1991), On the thermodynamics of the plasma sheet, *J. Geophys. Res.*, *96*, 20,991–20,998.
- Gombosi, T. I., and A. F. Nagy (1989), Time-dependent modeling of field-aligned current-generated ion transients in the polar wind, *J. Geophys. Res.*, *94*, 359–369.
- Kamide, Y., and S. Kokubun (1996), Two-component auroral electrojet: Importance for substorm studies, *J. Geophys. Res.*, *101*, 13,027–13,046.
- Kistler, L. M., E. Mobius, W. Baumjohann, G. Paschmann, and D. C. Hamilton (1992), Pressure changes in the plasma sheet during substorm injections, *J. Geophys. Res.*, *97*, 2973–2983.
- Korth, H., M. F. Thomsen, J. E. Borovsky, and D. J. McComas (1999), Plasma sheet access to geosynchronous orbit, *J. Geophys. Res.*, *104*, 25,047–25,061.
- Lui, A. T. Y. (1991), Extended consideration of a synthesis model for magnetospheric substorms, in *Magnetospheric Substorms*, *Geophys. Monogr. Ser.*, vol. 64, edited by J. R. Kan et al., pp. 43–60, AGU, Washington, D. C.
- Lyons, L. R., C.-P. Wang, T. Nagai, T. Mukai, Y. Saito, and J. C. Samson (2003a), Substorm inner plasma sheet particle reduction, *J. Geophys. Res.*, *108*(A12), 1426, doi:10.1029/2003JA010177.
- Lyons, L. R., C.-P. Wang, and T. Nagai (2003b), Substorm onset by plasma sheet divergence, *J. Geophys. Res.*, *108*(A12), 1427, doi:10.1029/2003JA010178.
- McPherron, R. L., C. T. Russell, and M. P. Aubry (1973), Satellite studies of magnetospheric substorms on August 15, 1968, 9, Phenomenological model for substorms, *J. Geophys. Res.*, *78*, 3131–3149.
- Opgenoorth, H. J., M. A. L. Persson, T. I. Pulkkinen, and R. J. Pellinen (1994), Recovery phase of magnetospheric substorms and its association with morning-sector aurora, *J. Geophys. Res.*, *99*, 4115–4129.
- Pulkkinen, T. I., and N. A. Tsyganenko (1996), Testing the accuracy of magnetospheric model field line mapping, *J. Geophys. Res.*, *101*, 27,431–27,442.
- Spence, H. E., and M. G. Kivelson (1993), Contributions of the low-latitude boundary layer to the finite width magnetotail convection model, *J. Geophys. Res.*, *98*, 15,487–15,496.
- Tsyganenko, N. A. (1989), A magnetospheric magnetic field model with a warped tail current sheet, *Planet Space Sci.*, *37*, 5–20.
- Wang, C.-P., L. R. Lyons, M. W. Chen, and F. R. Toffoletto (2004), Modeling the transition of the inner plasma sheet from weak to enhanced convection, *J. Geophys. Res.*, *109*, A12202, doi:10.1029/2004JA010591.
- Wilson, G. R., D. M. Ober, G. A. Germany, and E. J. Lund (2004), Night-side auroral zone and polar cap ion outflow as a function of substorm size and phase, *J. Geophys. Res.*, *109*, A02206, doi:10.1029/2003JA009835.
- Wing, S., and P. T. Newell (1998), Central plasma sheet ion properties as inferred from ionospheric observations, *J. Geophys. Res.*, *103*, 6785–6800.
- Wing, S., and P. T. Newell (2000), Quiet time plasma sheet ion pressure contribution to Birkeland currents, *J. Geophys. Res.*, *105*, 7793–7802.
- Winglee, R. M., W. Lewis, and G. Lu (2005), Mapping of the heavy ion outflows as seen by IMAGE and multifluid global modeling for the 17 April 2002 storm, *J. Geophys. Res.*, *110*, A12S24, doi:10.1029/2004JA010909.
- Wolf, R. A., V. Kumar, F. R. Toffoletto, G. M. Erickson, A. M. Savoie, C. X. Chen, and C. L. Lemon (2006), Estimating local plasma sheet $PV^{5/3}$ from single-spacecraft measurements, *J. Geophys. Res.*, *111*, A12218, doi:10.1029/2006JA012010.

J. W. Gjerloev and S. Wing, Johns Hopkins University Applied Physics Laboratory, Laurel, MD 20723, USA. (simon.wing@jhuapl.edu)
 R. A. Hoffman, Space Weather Laboratory, NASA Goddard Space Flight Center, Greenbelt, MD 20771, USA.
 J. R. Johnson, Princeton Plasma Physics Laboratory, Princeton, NJ 08543, USA.